THE ASTROPHYSICAL JOURNAL, 461:847–857, 1996 April 20

THE EFFECT OF MULTIPLE SCATTERING ON THE POLARIZATION FROM AXISYMMETRIC CIRCUMSTELLAR ENVELOPES. II. THOMSON SCATTERING IN THE PRESENCE OF ABSORPTIVE OPACITY SOURCES

KENNETH WOOD, J. E. BJORKMAN, BARBARA WHITNEY, AND ARTHUR CODE
Department of Astronomy, University of Wisconsin, 475 North Charter Street, Madison, WI 53706
Received 1995 August 28; accepted 1995 October 26

ABSTRACT

We investigate the effect on the polarization of multiple Thomson scattered stellar radiation in axisymmetric circumstellar envelopes that contain sources of continuous absorptive opacity and emission. Our previous investigations of pure electron scattering envelopes have shown that multiple scattering increases the polarization level above that predicted by single scattering plus attenuation approximations. However, the inclusion of sources of absorptive opacity within the envelope lowers the albedo, reducing the number of multiply scattered photons. Consequently, for envelopes possessing a large absorptive opacity, the net polarization approaches the single-scattering plus attenuation levels (which may be positive or negative, depending on the geometry and degree of polarimetric cancellation). Lowering the albedo further (by increasing the absorptive opacity) removes photons that have been singly scattered so that the polarization decreases below that predicted by the single-scattering plus attenuation approximation. As the albedo approaches zero, few photons are scattered within the envelope (all are absorbed), and the only radiation reaching the observer is unscattered (i.e., unpolarized) stellar radiation; hence, the polarization approaches zero.

A consequence of this behavior is that when the albedo changes rapidly with wavelength, as occurs across ionization edges (e.g., across the Balmer jump), much larger changes in the polarization occur than predicted by single-scattering plus attenuation approximations. This occurs because just shortward of the jump, the absorptive opacity is large (effective albedo is small), and the polarization approaches the single-scattering plus attenuation level (since many multiply scattered photons have been absorbed). However, just longward of the jump, where the absorptive opacity is small (effective albedo is close to unity), multiple scattering is dominant, and the polarization is larger than the single scattering plus attenuation prediction. For this reason we find that the combined effects of multiple scattering plus absorptive opacity give much larger polarization jumps than previous predictions; in some instances, the polarization jump is doubled. In addition, the slope of the polarized continuum is steeper than that derived from single scattering plus attenuation calculations. Finally, for geometrically thick equatorial disk–like geometries, a position angle flip of 90° occurs shortward of the Balmer jump. This is because of the large hydrogen opacity which absorbs the multiply scattered photons in the equatorial disk. Thus, the polarization is dominated by singly scattered photons from the polar regions, producing a net negative polarization.

Subject headings: circumstellar matter — methods: numerical — polarization — radiative transfer — scattering

1. INTRODUCTION

In a previous Monte Carlo investigation (Wood et al. 1996, hereafter Paper I), we demonstrated that multiple scattering of stellar radiation within an axisymmetric circumstellar envelope yields polarization levels that are higher than those predicted by "single-scattering plus attenuation" approximations (e.g., Fox 1994; Bjorkman & Bjorkman 1994). The reason for the higher polarization levels is that multiply scattered photons are confined to scatter in the plane of the disk. Multiple scattering in a single plane reduces the component of the electric vector parallel to the plane, leaving the perpendicular component unaltered. Thus, the polarization (the difference between the two orthogonal components divided by the sum of the components) is increased above the single scattering results. In Paper I we considered pure electron scattering circumstellar envelopes, which produce a polarization spectrum that is independent of wavelength. However, spectropolarimetric observations of Be stars (e.g., Bjorkman et al. 1991) and other unresolved stellar systems show a wavelength dependence to the intrinsic continuum polarization. These variations are attributed to additional absorptive opacity sources within the circumstellar envelope which change the envelope albedo, reducing the multiple scattering and thus modifying the emergent polarized spectrum. In Be stars, the additional absorptive opacity is attributed to continuous hydrogen opacity in the visible, free-free opacity in the IR, and metal line blanketing in the UV.

In this paper we present results of Monte Carlo calculations that show the effect of continuous absorption on the polarization by varying the scattering albedo in various axisymmetric circumstellar envelopes. As with all Monte Carlo calculations, we are only able to investigate specific geometries. To maintain some diversity and to illustrate the general effects that the scattering albedo has on the emergent continuum polarization, in § 2 we investigate the effects of varying the scattering albedo in geometrically thin and geometrically thick circumstellar disks. For each disk geometry we consider two different optical depth regimes (one small and one large) and find as a result of polarization

sign reversals at large equatorial optical depths that the polarization can vary with albedo in a complex manner. For circumstellar disks of small optical depth, the polarization decreases with decreasing albedo. For small albedos, the multiply scattered photons are all absorbed, and the polarization agrees with the single-scattering plus attenuation approximation.

In § 3 we investigate the effects of continuous hydrogen absorptive opacity on the emergent polarized spectrum. In addition to stellar photons, we also include the electron scattering of the envelope emission from free-bound and free-free processes. We find that, in addition to the increased polarization arising from multiple scattering in the envelope, departures from the single-scattering plus attenuation approximation are most pronounced across absorption edges (e.g., the Balmer and Paschen jumps), where the effective albedo changes rapidly with wavelength.

2. VARYING THE ALBEDO IN CIRCUMSTELLAR DISKS

In this section we calculate the polarization arising from multiple scattering in axisymmetric circumstellar envelopes in which the scattering albedo is not unity. The albedo for Thomson scattering is one, so varying the albedo is equivalent to introducing additional absorptive opacity sources in the envelope (see § 3). We investigate circumstellar disk–like geometries in which the electron number density is parameterized by

$$n_e = n_0\left(\frac{R_*}{r}\right)^n (1 + A \sin^m \theta) , \qquad (1)$$

where $(1 + A)$ is the equatorial to polar density ratio, m determines the opening angle of the disk, and n is the radial exponent of the density distribution. This density parameterization enables us to investigate geometrically thin disks (large m values) with large equator-to-pole density ratios (i.e., large A values). Such disks have been predicted to form around rapidly rotating Be stars (Bjorkman & Cassinelli 1993; Owocki, Cranmer, & Blondin 1994). Less oblate circumstellar geometries (i.e., small m and A values) have been postulated to surround Wolf-Rayet stars (Cassinelli, Ignace, & Bjorkman 1994; Ignace, Cassinelli, & Bjorkman 1996); the parameterization of equation (1) conveniently enables us to investigate these geometries as well. In the following sections, we investigate the effect on the polarization of varying the scattering albedo in both geometrically thin and geometrically thick circumstellar disks. The albedo effects are incorporated into the Monte Carlo analysis by generating a pseudorandom number (between 0 and 1) after the photon travel distance has been calculated. If this pseudorandom number is greater than the scattering albedo, the photon is terminated (i.e., absorbed) and a new photon is emitted; otherwise, the photon is scattered and followed until it is either absorbed or escapes from the envelope (see the description in § 3.1 of Paper I).

2.1. *Geometrically Thin Equatorial Disk*

The disk density is given by equation (1) with $A = 99$, $m = 500$, and $n = 3$ and is illustrated in Figure 1. This is a disk with an equatorial-to-polar density ratio of 100 and an opening angle (measured from the equator) of 3°. In Figures

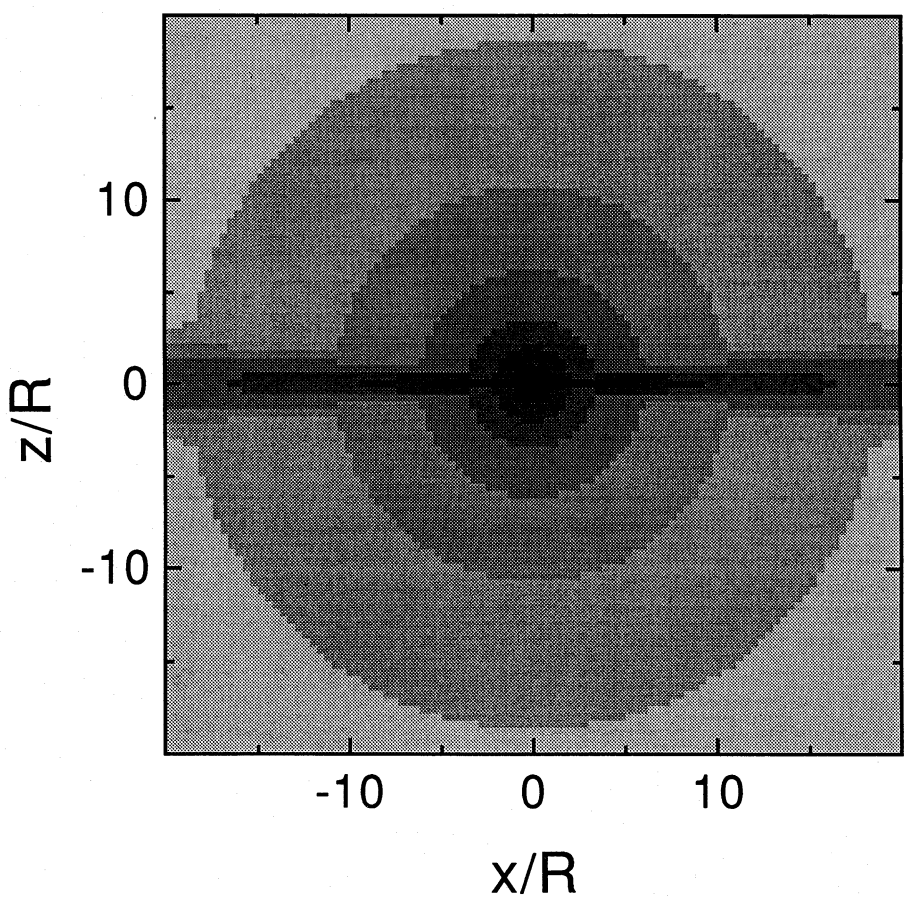

FIG. 1.—Gray-scale density plot of a geometrically thin disk. The equatorial-to-polar density ratio is 100, and the disk opening angle is 3°.

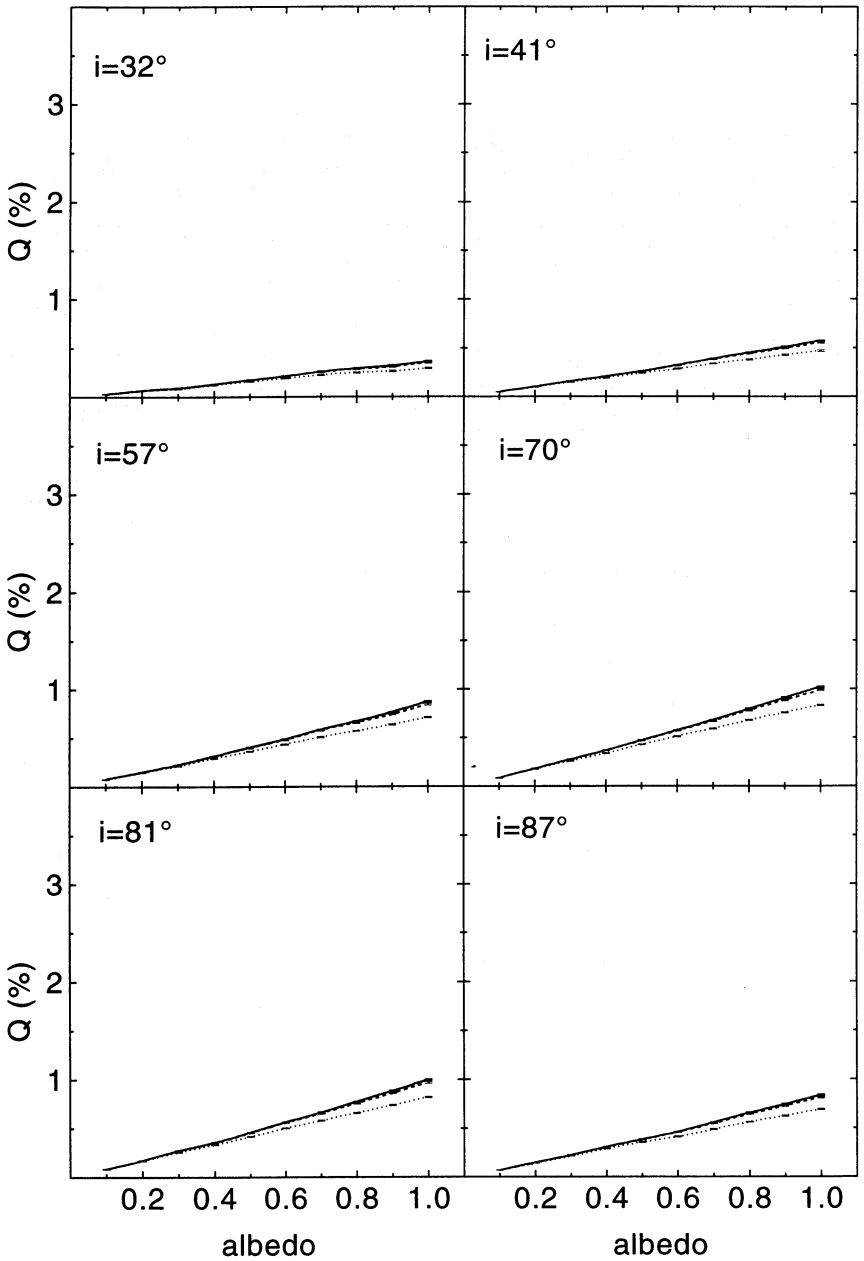

FIG. 2*a*

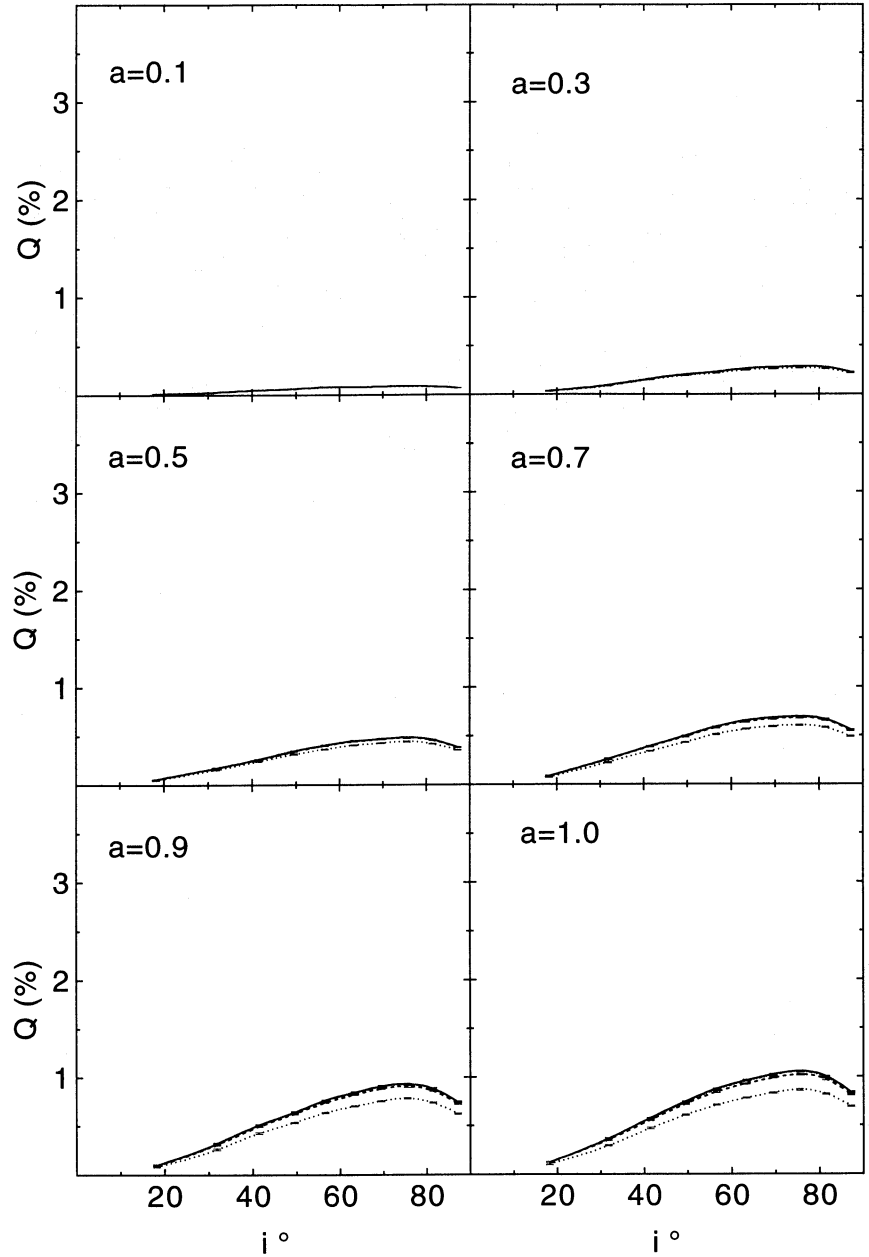

FIG. 2*b*

FIG. 2.—(*a*) Polarization as a function of albedo for various inclination angles arising from scattering radiation in the circumstellar disk of Fig. 1. The equatorial optical depth of the disk is $\tau_{eq} = 1$. The dotted line is the single-scattered polarization, the dashed line is for polarization arising from photons that have been scattered up to two times, the dot-dashed line is for photons that have been scattered up to three times, and the solid line is the polarization arising from all scatterings. (*b*) Polarization as a function of inclination for various albedos arising from scattering radiation in the circumstellar disk of Fig. 1. The equatorial optical depth of the disk is $\tau_{eq} = 1$. The line types are same as in (*a*).

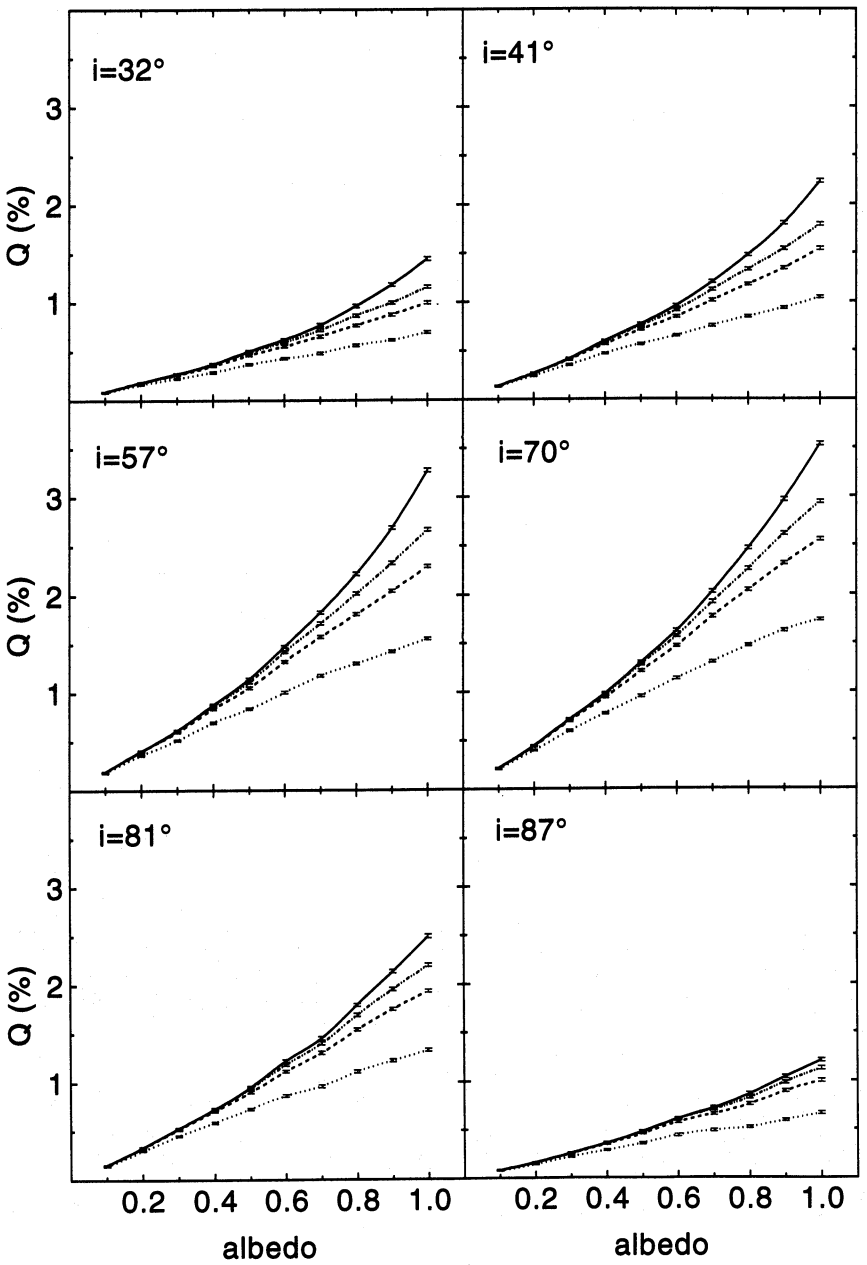

FIG. 3*a*

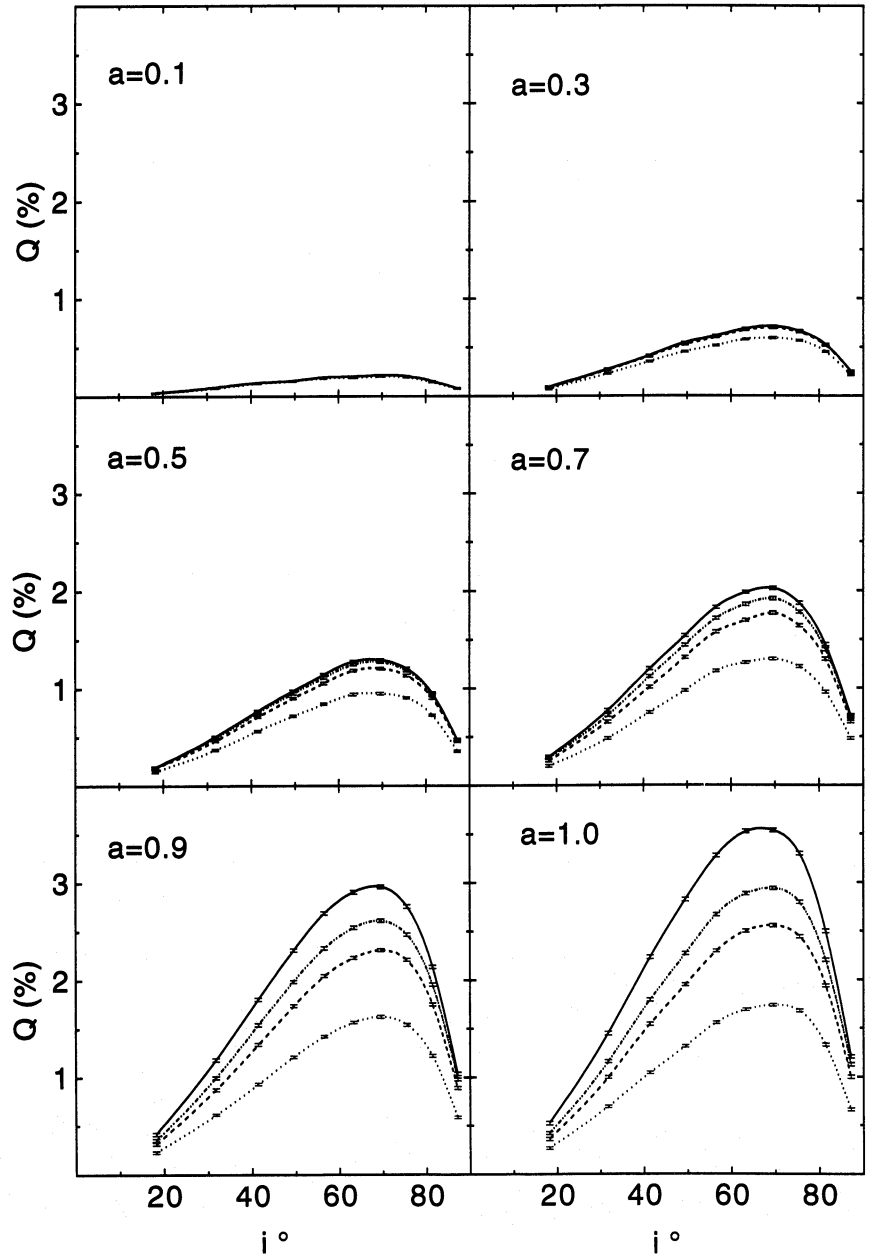

FIG. 3*b*

FIG. 3.—(*a*) Same as Fig. 2*a*, but for an equatorial optical depth of $\tau_{eq} = 10$. (*b*) Same as Fig. 2*b*, but for an equatorial optical depth of $\tau_{eq} = 10$.

2 and 3 we show the results of our Monte Carlo polarization calculations for this disk. These figures show the variation in polarization with scattering albedo for different inclinations of this geometrically thin circumstellar disk. Figures 2*a* and 2*b* show the results for such a disk with a small equatorial optical depth ($\tau_{eq} = 1$), while Figures 3*a* and 3*b* show the results for an equatorial optical depth $\tau_{eq} = 10$. It is seen that, for the disk of small optical depth, the polarization is dominated by single-scattered photons, and the polarization declines with decreasing albedo. Lowering the albedo removes scattered photons, thus reducing the net polarization. For the $\tau_{eq} = 10$ case shown in Figures 3*a* and 3*b*, we see for an albedo of 1 that multiple scattering has a large effect on the polarization; for some inclinations, the polarization is doubled compared to the single-scattered photon polarization. As the albedo is lowered, the multiple-scattering polarization approaches the single-scattering results. This occurs because lowering the albedo reduces the number of multiple scatterings that occur within the circumstellar disk; thus, the single and multiple scattering curves converge. It is seen that for an albedo less than 0.5, the polarization is dominated by single-scattered photons. Further reducing the albedo removes even these single-scattered photons, so the polarization eventually approaches zero as the albedo becomes very small. The scattering statistics for these two cases are shown in Tables 1A and 1B. Note that for the optically thick disk, a larger percentage of photons are scattered and absorbed than for the optically thin case. Note also that the polarization is always positive, since no polar cancellation occurs for this geometrically thin disk with a high equatorial-to-polar density ratio. Consequently the polarization variation for this case is relatively simple. However, as we shall see in the next section, when polar cancellation effects are important the polarization variation with albedo takes a more complex form.

2.2. *Geometrically Thick Equatorial Disk*

In this section we present the polarization produced by a geometrically thick disk with a small equator-to-pole density ratio. The disk density, illustrated in Figure 4, is given by equation (1) with $A = 4$, $m = 4$, and $n = 3$. These parameters produce an equator-to-pole density ratio of 5 and an opening angle of 33°. Figures 5*a* and 5*b* show the results for an optically thin disk ($\tau_{eq} = 1$), and Figures 6*a* and 6*b* show the $\tau_{eq} = 5$ case. The optically thin results (Figs. 5*a* and 5*b*) are similar to those of Figures 2*a* and 2*b* and show the polarization decreasing with decreasing albedo. Note that the overall polarization level is higher than for the geometrically thin disk, since more photons are scattered and become polarized. This is evident by comparing the bookkeeping table for this case (Table 2A) with that for the geometrically thin disk (Table 1A): the percentage of scattered photons is higher for the geometrically thick disk.

Figures 6*a* and 6*b* show the polarization from the high optical depth disk. Note that the variation with albedo is very different from any of the previous figures. For this geometry, with an albedo of one, there is a significant amount of polar cancellation occurring, and the single-scattered polarization is negative; i.e., most single-scattered

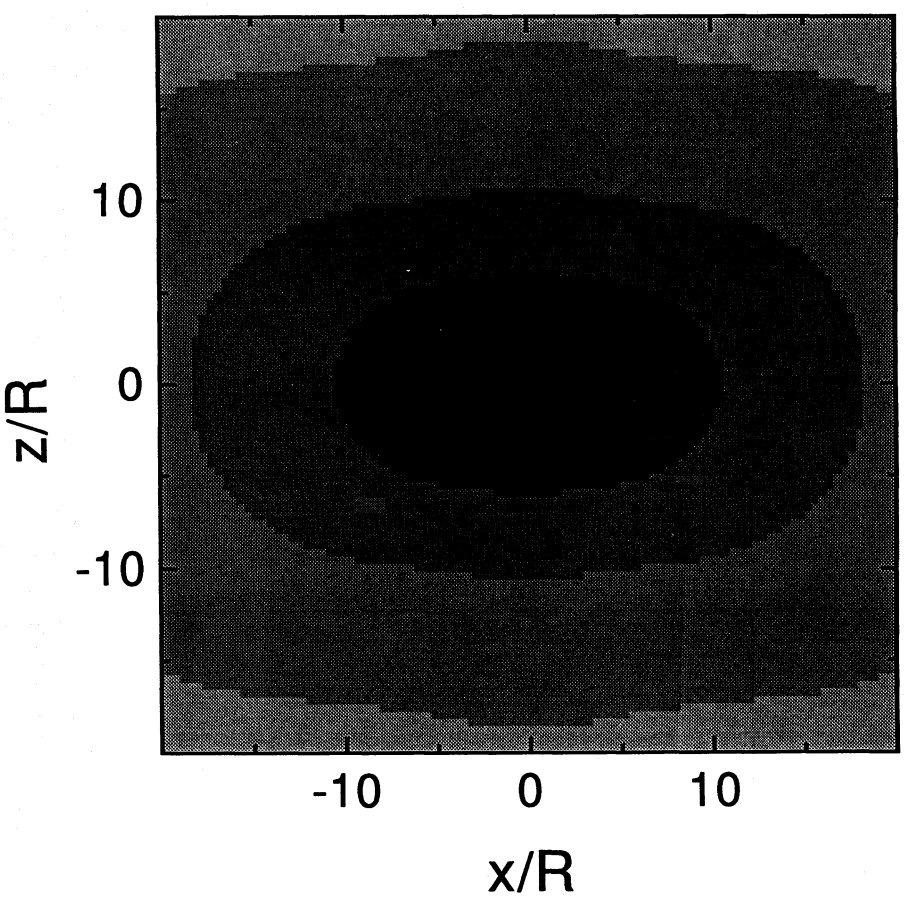

FIG. 4.—Gray-scale density plot of a geometrically thick disk. The equatorial-to-polar density ratio is 5, and the disk opening angle is 33°.

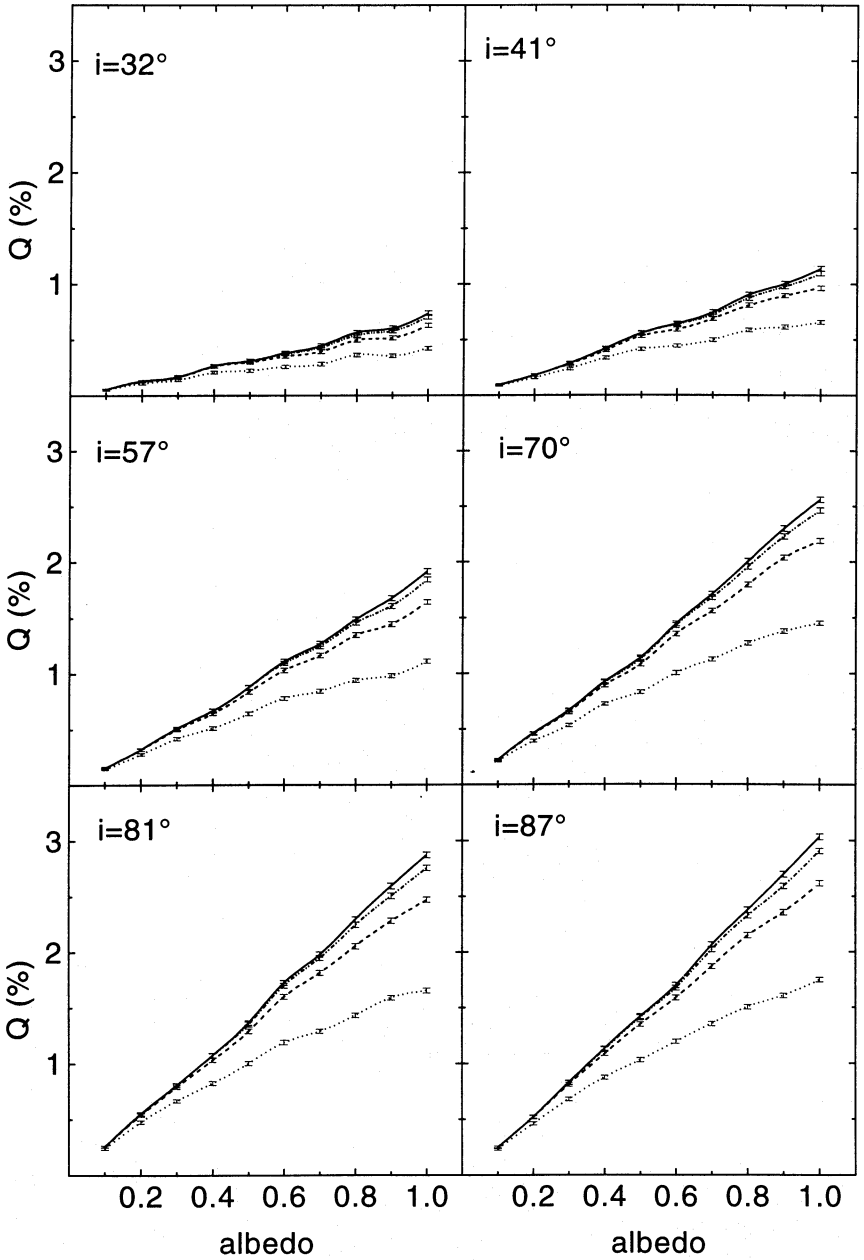

FIG. 5a

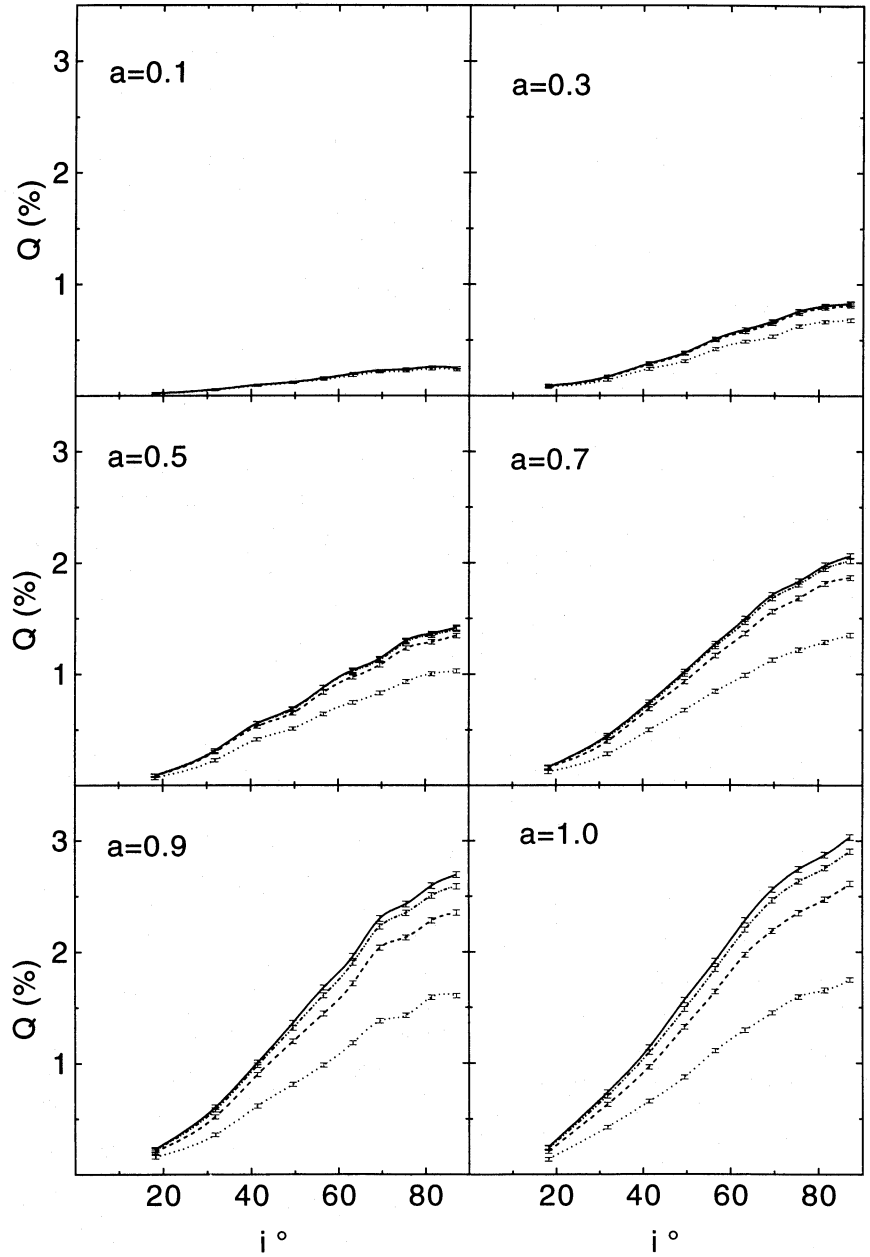

FIG. 5b

FIG. 5.—(*a*) Polarization as a function of albedo for various inclination angles arising from scattering radiation in the circumstellar disk of Fig. 4. The equatorial optical depth of the disk is $\tau_{eq} = 1$. The line types are the same as in Fig. 2*a*. (*b*) Polarization as a function of inclination for various albedos arising from scattering radiation in the circumstellar disk of Fig. 1. The equatorial optical depth of the disk is $\tau_{eq} = 1$. The line types are the same as in Fig. 2*a*.

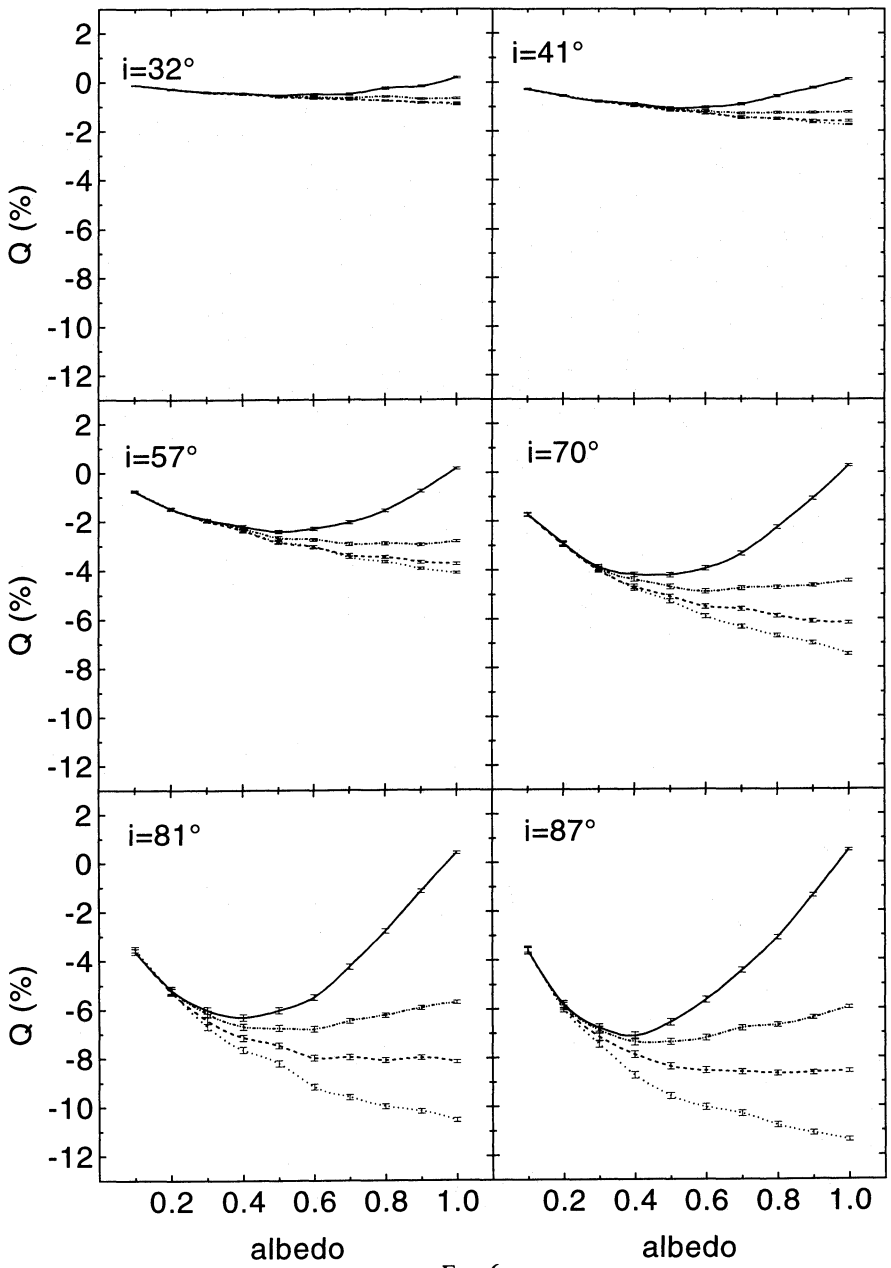

FIG. 6*a*

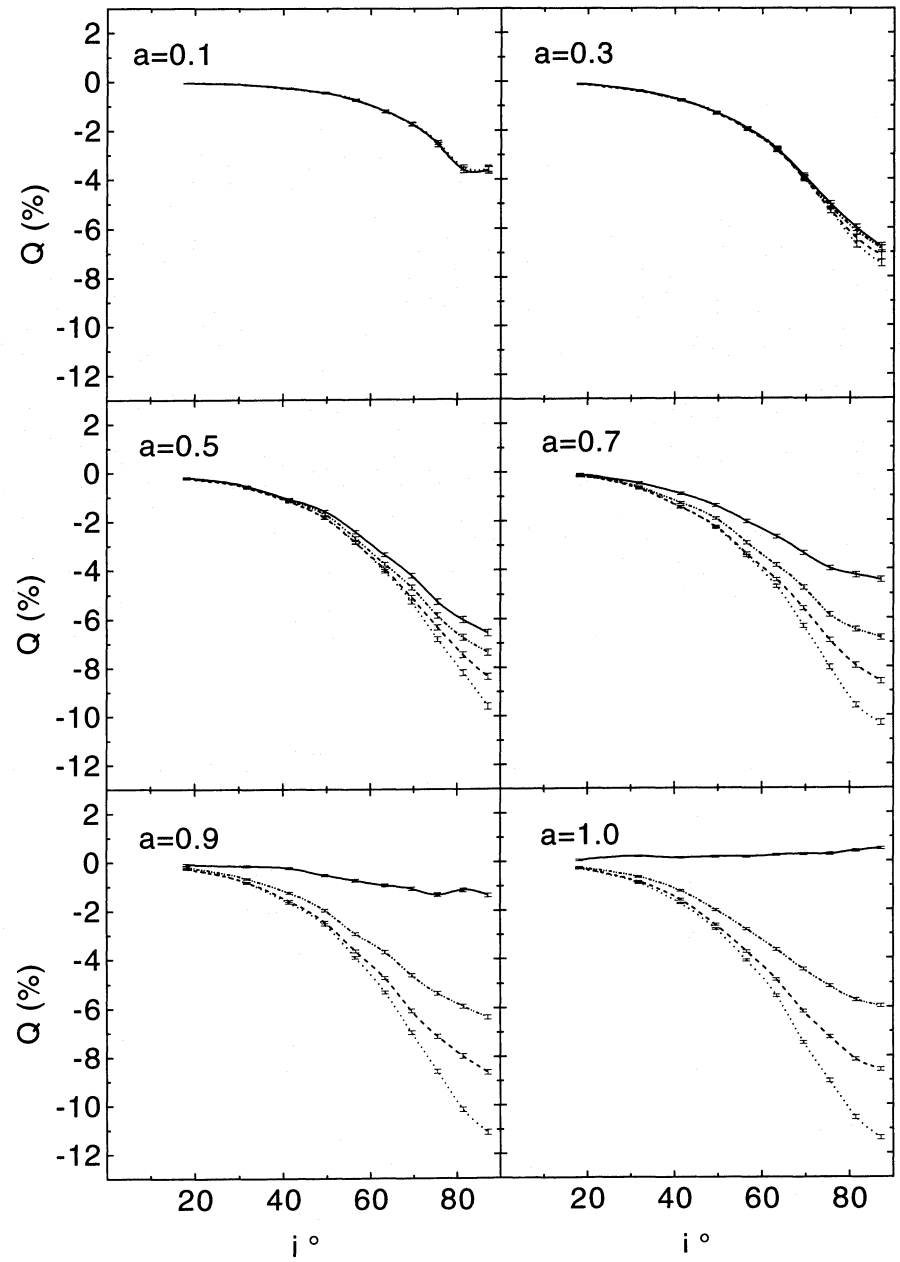

FIG. 6*b*

FIG. 6.—(*a*) Same as Fig. 5*a*, but for an equatorial optical depth of $\tau_{eq} = 5$. (*b*) Same as Fig. 5*b*, but for an equatorial optical depth of $\tau_{eq} = 5$.

TABLE 1

PERCENTAGE OF UNSCATTERED, SCATTERED, AND ABSORBED PHOTONS AND THE AVERAGE NUMBER OF SCATTERINGS PER SCATTERED PHOTON FOR THE GEOMETRY ILLUSTRATED IN FIGURE 1

A. $\tau_{eq} = 1$

Albedo	Unscattered Photons (%)	Scattered Photons (%)	Absorbed Photons (%)	Average Number of Scatterings
0.1.....	93.27	0.49	6.24	1.01
0.2.....	93.39	0.97	5.64	1.02
0.3.....	93.52	1.48	5.00	1.04
0.4.....	93.65	2.00	4.35	1.05
0.5.....	93.78	2.54	3.68	1.07
0.6.....	93.93	3.08	2.99	1.08
0.7.....	94.07	3.65	2.28	1.10
0.8.....	94.20	4.25	1.55	1.11
0.9.....	94.37	4.85	0.78	1.13
1.0.....	94.52	5.48	0.00	1.15

B. $\tau_{eq} = 10$

Albedo	Unscattered Photons (%)	Scattered Photons (%)	Absorbed Photons (%)	Average Number of Scatterings
0.1.....	68.70	1.30	30.00	1.04
0.2.....	69.03	2.73	28.24	1.09
0.3.....	69.40	4.31	26.29	1.14
0.4.....	69.80	6.06	24.14	1.21
0.5.....	70.26	8.03	21.71	1.28
0.6.....	70.78	10.30	18.92	1.39
0.7.....	71.41	12.96	15.63	1.52
0.8.....	72.15	16.15	11.70	1.69
0.9.....	73.11	20.18	6.71	1.95
1.0.....	74.37	25.63	0.00	2.35

TABLE 2

PERCENTAGE OF UNSCATTERED, SCATTERED, AND ABSORBED PHOTONS AND THE AVERAGE NUMBER OF SCATTERINGS PER SCATTERED PHOTON FOR THE GEOMETRY ILLUSTRATED IN FIGURE 4

A. $\tau_{eq} = 1$

Albedo	Unscattered Photons (%)	Scattered Photons (%)	Absorbed Photons (%)	Average Number of Scatterings
0.1.....	49.67	2.21	48.12	1.05
0.2.....	50.16	4.66	45.18	1.10
0.3.....	50.75	7.43	41.82	1.15
0.4.....	51.36	10.56	38.08	1.22
0.5.....	52.04	14.11	33.85	1.28
0.6.....	52.83	18.20	28.97	1.36
0.7.....	53.71	22.90	23.39	1.45
0.8.....	54.72	28.44	16.84	1.55
0.9.....	55.85	34.98	9.17	1.66
1.0.....	57.21	42.79	0.00	1.79

B. $\tau_{eq} = 5$

Albedo	Unscattered Photons (%)	Scattered Photons (%)	Absorbed Photons (%)	Average Number of Scatterings
0.1.....	5.48	0.63	93.89	1.10
0.2.....	5.62	1.45	92.93	1.22
0.3.....	5.78	2.50	91.72	1.37
0.4.....	5.94	3.94	90.12	1.56
0.5.....	6.18	5.94	87.88	1.80
0.6.....	6.46	8.87	84.67	2.13
0.7.....	6.87	13.51	79.62	2.60
0.8.....	7.44	21.63	70.92	3.31
0.9.....	8.44	38.55	53.01	4.55
1.0.....	10.77	89.23	00.00	7.25

photons are from the negatively polarized polar regions. However, the multiple-scattered polarization is still positive, indicating that multiple scattering occurs within the equatorial regions. As the albedo is lowered, the negative single-scattered polarization decreases, while the actual polarization (arising from the multiply scattered photons) decreases also with decreasing albedo. However, there is a sign reversal of the polarization when the albedo is below about 0.8. This occurs because the polarization is now dominated by photons that have only been scattered once or twice within the circumstellar envelope (i.e., all the higher order scatterings have been absorbed). Since most of the single- and double-scattered photons reach the observer from the polar regions, the net polarization is negative. The effect produces the seemingly complex polarization variation with albedo in which the polarization begins positive, decreases to a negative maximum (minimum), and then increases back to zero. Similar variations were discovered by Hillier (1994), who calculated the polarization from mildly prolate plumes in which significant polarization cancellation occurred, yielding polarization variations with albedo that swung both positive and negative. At the time these variations were somewhat confusing, but they are now relatively straightforward to understand when we realize that the multiple- and single-scattered polarization curves converge as the albedo is reduced. This fact is clearly demonstrated by the individual curves in all the above figures that show the polarization arising from photons that have been scattered once, those that have been scattered up to two times, those that have undergone up to three scatterings, and finally the polarization resulting from all scatterings within the circumstellar envelope.

3. POLARIZATION FROM PURE HYDROGEN CIRCUMSTELLAR DISKS

The results of § 2 imply that a wavelength dependence of the albedo will yield spectral slopes of the polarized continuum that are different than the single-scattering approximations and that the most pronounced differences will occur when the albedo changes rapidly with wavelength, such as across absorption edges. We now investigate the polarization arising from circumstellar envelopes that contain wavelength-dependent absorptive opacity sources. In particular, we will consider a pure hydrogen disk.

Bjorkman & Bjorkman (1994) investigated the polarization arising from Be circumstellar disks (parameterized by eq. [1]) in the single-scattering plus attenuation approximation. In their calculation, the polarization arose due to single Thomson scattering of stellar radiation in the disk with an optical depth correction factor, $e^{-\tau}$, included to account for both attenuation (due to continuous hydrogen absorptive opacity) and electron scattering of radiation out of the line of sight. The wavelength dependence of the hydrogen opacity is given by

$$\rho\kappa_\nu = a_{\rm ff}\left[1 - \exp\left(-\frac{h\nu}{kT}\right)\right]\frac{n_e^2}{\nu^3 T^{1/2}} + \begin{cases} n_2\, a_2(\nu_2/\nu)^3 + n_3\, a_3(\nu_3/\nu)^3 & (\nu > \nu_2)\,, \\ n_3\, a_3(\nu_3/\nu)^3 & (\nu_2 > \nu > \nu_3)\,, \end{cases} \quad (2)$$

where the first term arises from free-free absorption and the second arises from bound-free absorption. The free-free absorption coefficient is $a_{\rm ff} = 3.692 \times 10^8$ cm^5 s^{-3} K$^{1/2}$,

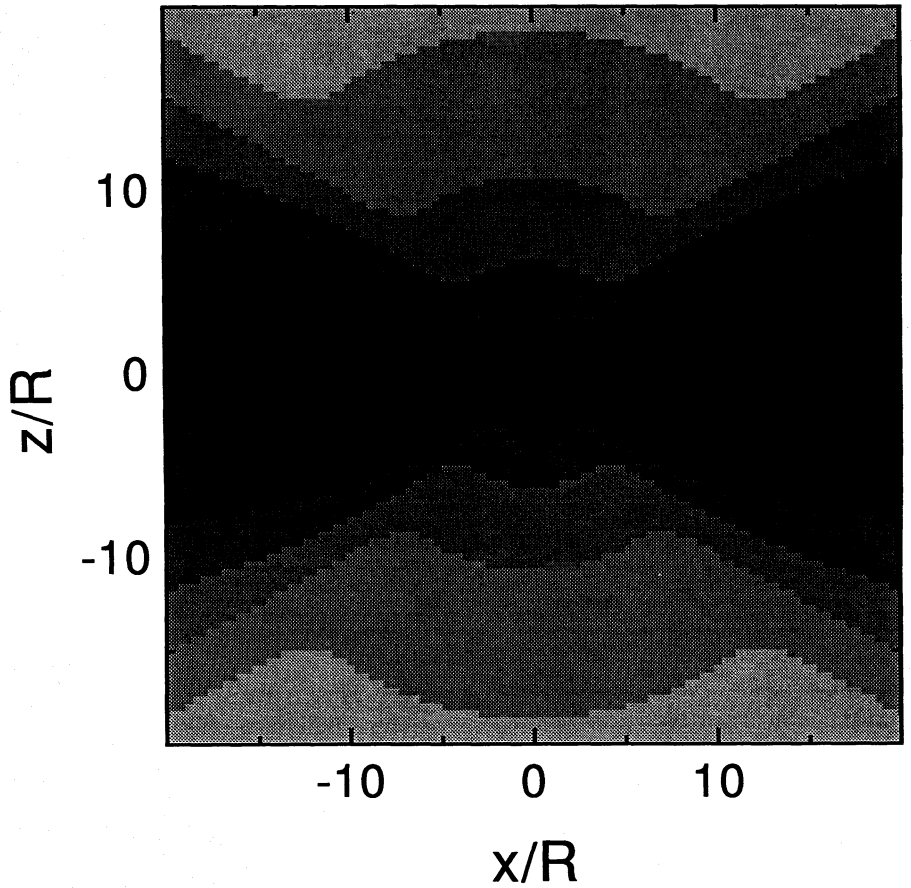

FIG. 7.—Gray-scale plot of the circumstellar geometry used for the polarization calculations shown in Fig. 8. The equatorial-to-polar density ratio is 1000, and the disk opening angle is 15°.

and the photoionization cross sections are $a_2 = 1.4 \times 10^{-17}$ cm^2 and $a_3 = 2.2 \times 10^{-17}$ cm^2 at the Balmer and Paschen thresholds ν_2 and ν_3, respectively. The level populations were determined from a non-LTE approximation of Cassinelli, Nordsieck, & Murison (1987) and are given by

$$n_i^{\rm H} = \frac{q_i n_e^2}{W} \; (i = 2, 3) \, , \tag{3}$$

where $W = 0.5\{1 - [1 - (r/R)^2]^{1/2}\}$ is the dilution factor. The proportionality constant, q_i, is determined by matching the average excitations shown in Figure 3 of Cassinelli et al. (1987), which presents the results of a detailed non-LTE calculation. Bjorkman & Bjorkman investigated a B2 star ($T_{\rm eff} = 20{,}000$ K) and derived $q_2 = 3.5 \times 10^{-21}$ cm^3 and $q_3 = 4.7 \times 10^{-22}$ cm^3.

In addition to stellar radiation, they included free-free and free-bound disk emission, but only as a diluting agent, and they did not account for the scattering of this diffuse radiation field (in the same manner as Waters & Marlborough 1992). The envelope emissivity at each wavelength is given by

$$j_\nu = \frac{1}{4\pi} \gamma_\nu({\rm H}^0, T) n_e^2 \, , \tag{4}$$

where the values of $\gamma_\nu({\rm H}^0, T)$ are given in Table 4.7 in Osterbrock (1989). In our Monte Carlo simulation, the effects of scattering of this diffuse disk emission are included.

3.1. *Geometrically Thin Circumstellar Disk*

To compare our results with those of Bjorkman & Bjorkman, the first geometry we consider is a disk parameterized by equation (1) with $A = 999$, $m = 10$, $n = 3$, and an equatorial electron scattering optical depth of $\tau_{\rm eq} = 1.5$. This model is a disk with opening angle of 15° and an equatorial-to-polar density ratio of 1000, shown in Figure 7. In Figure 8 we show the results of our Monte Carlo simulation of this system, in which we include multiple scattering of stellar and disk radiation. We show the polarization, as a function of wavelength, arising from photons that have been scattered once, up to two times, up to three times, and finally the polarization arising from all scatterings of stellar and disk photons. It is seen that the multiple scattering increases the polarization above the single-scattering level (as expected). In addition to this effect, we find that as the continuous hydrogen absorptive opacity varies with wavelength, the slope of the continuum polarization changes from the single-scattering predictions and the size of the polarization Balmer jump increases. These effects may be explained as follows.

Just shortward of the Balmer jump, the hydrogen opacity is large (i.e., effective albedo is small), so multiply scattered photons are absorbed and the polarization approaches the single scattering results (see Fig. 8). Just longward of the jump, the hydrogen opacity is small (i.e., effective albedo is close to unity), and multiple scattering dominates the polarization, increasing the level above that of the single-

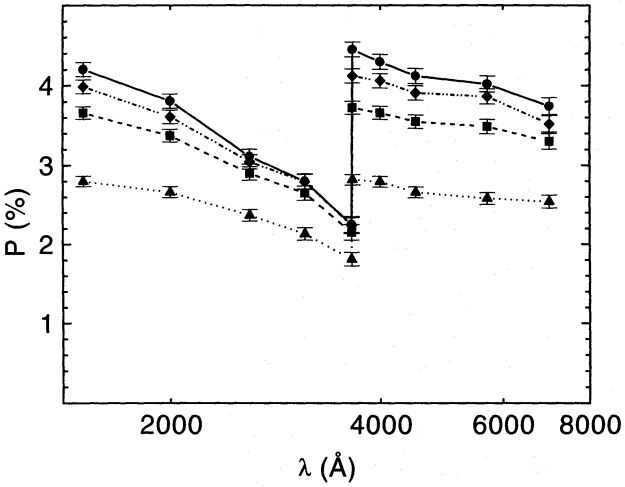

FIG. 8.—Polarization spectrum arising from scattering and absorption of stellar and free-free disk radiation in the circumstellar geometry (viewed edge-on) shown in Fig. 7. The spectral variations in the degree of polarization are caused by absorption by continuous hydrogen opacity. Note that the actual polarization Balmer jump is larger than that predicted from single scattering theory. The line types are the same as in Fig. 2*a*.

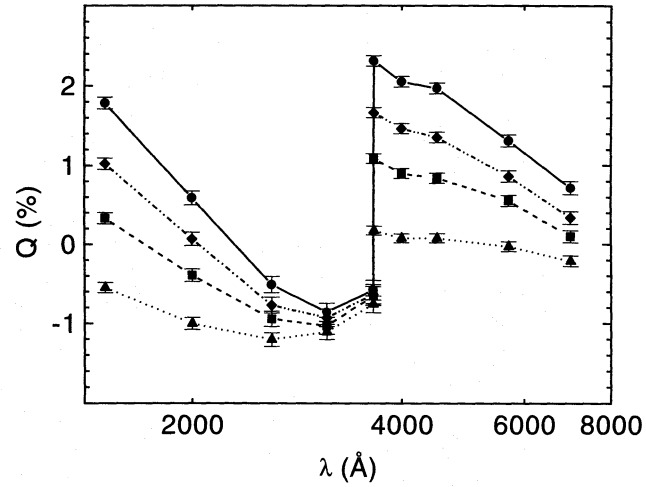

FIG. 9.—Same as Fig. 8, except for the geometrically thick circumstellar geometry of Fig. 4 (viewed edge-on). Note that the polarization is negative just shortward of the Balmer jump. This is because of the large hydrogen opacity absorbing photons that are multiply scattered in the disk, leaving the net polarization dominated by polar single-scattered (negatively polarized) photons. The line types are the same as in Fig. 2*a*.

scattered photons. This effect increases the size of the polarization jumps so that they are larger than predicted by a single scattering plus attenuation analysis. As the wavelength increases longward of the jump, the hydrogen opacity increases also, so the multiply scattered photons are increasingly absorbed and the net polarization begins to converge to the single scattering results. This effect increases the slope of the continuum polarization above that obtained from a single scattering plus attenuation analysis.

3.2. *Geometrically Thick Circumstellar Disk*

We consider now a geometrically thick disk shown in Figure 4. This disk has an equator-to-polar density ratio of 5 and an opening angle of 33°, following Bjorkman & Bjorkman (1994). We choose the equatorial electron scattering optical depth to be $\tau_{eq} = 0.5$. The results of our Monte Carlo simulation of this system are shown in Figure 9. It is seen that shortward of the Balmer jump the polarization is negative (i.e., the position angle has flipped by 90°). This can be explained by considering the polarization versus albedo results for this geometry presented in Figure 6. Owing to polar cancellation and the removal of multiple-scattered photons, the polarization is negative for small albedos. This situation occurs shortward of the Balmer jump, where the hydrogen absorptive opacity is large (i.e., effective albedo is small), so that the multiple-scattered photons are absorbed, leaving the polarization dominated by photons that are scattered in the negatively polarized polar regions. For very short wavelengths, the hydrogen absorption is small and the polarization is once again positive: photons that are multiply scattered in the disk dominate the polarization. Note that the signature of this effect is two position angle flips; gravity darkening only produces one position angle flip.

4. CONCLUSIONS

In this paper we have investigated the manner in which the continuum polarization from unresolved circumstellar disks varies with the scattering albedo. For geometrically thin disks, with large equatorial-to-polar density ratios, we find that decreasing the albedo reduces the polarization level. This is because the multiply scattered photons are preferentially absorbed, so the residual polarization at low albedos is dominated by single-scattered photons. For geometrically thick disks, with low equator-to-pole density ratios, the polarization can be negative for small values of the albedo. This occurs because in these disks there is significant cancellation of the positively polarized photons (scattered in the equatorial regions) by the negatively polarized photons that are scattered in the polar regions. Lowering the albedo reduces the polarization, and eventually the polarization is dominated by single- and double-scattered photons that are negatively polarized, hence the negative polarization at low albedos.

In our investigation of the effects on the continuum polarization of wavelength-dependent continuous absorption, we find that there are three major differences with our multiple-scattering calculation compared to the single-scattering plus attenuation approximation. The first is that the overall polarization level is higher because the multiple scattering is confined to a plane (as described in Paper I). The second is that the slope of the polarized continuum is steeper because the multiple-scattering polarization decreases to the single-scattering level as the effective albedo decreases, thereby increasing the slope. Finally, the polarization Balmer jump is much larger than single-scattering predictions. Multiple scattering is suppressed at wavelengths just shortward of the jump at which the albedo is low, while it is dominant just longward of the jump where the hydrogen absorptive opacity is small (i.e., effective albedo is close to unity). This sudden change in the albedo greatly increases the size of the polarization jump.

This investigation demonstrates again that the polarization levels observed in Be stars can be obtained easily with geometrically thin disks. In addition, the multiple-scattering plus albedo effects enable the formation of large jumps in, and steeper slopes of the polarized continuum, which may prove to be crucial in observational testing of circumstellar models of Be stars. For geometrically thick disks that have significant polar cancellation of the disk polarization, we find that there can be a position angle flip of 90° (i.e., negative polarization) shortward of the Balmer jump. This is

again an albedo effect whereby the removal of photons that are multiply scattered in the disk allows the domination of the negatively polarized polar photons. The fact that these position angle flips are not observed in Be stars may be an indication that Be circumstellar geometries are not mildly oblate. We are currently conducting a detailed investigation into the different polarization characteristics of geometrically thick and thin disks and the extent to which spectropolarimetric modeling can be used to determine the circumstellar geometry. These results will be presented in a future paper.

This work has been supported by a UK SERC/NATO postdoctoral research fellowship (K. W.), NSF grant AST 91-15375, and NASA grant NAGW-2921 (J. E. B.).

REFERENCES

Bjorkman, J. E., & Bjorkman, K. S. 1994, ApJ, 436, 818
Bjorkman, J. E., & Cassinelli, J. P. 1993, ApJ, 409, 429
Bjorkman, K. S., et al. 1991, ApJ, 383, L67
Cassinelli, J. P., Ignace, R., & Bjorkman, J. E. 1994, in IAU Symp. 163, Wolf-Rayet Stars: Binaries, Colliding Winds, Evolution, ed. K. A. van der Hucht & P. M. Williams (Dordrecth: Kluwer), 191
Cassinelli, J. P., Nordsieck, K. H., & Murison, M. A. 1987, ApJ, 317, 290
Fox, G. K. 1994, ApJ, 435, 372
Hillier, D. J. 1994, A&A, 289, 492
Ignace, R., Cassinelli, J. P., & Bjorkman, J. E. 1996, ApJ, 459, 671
Osterbrock, D. E. 1989, AGN^2 (Mill Valley, CA: University Science Books)
Owocki, S. P., Cranmer, S. R., & Blondin, J. M. 1994, ApJ, 424, 887
Waters, L. B. F. M., & Marlborough, J. M. 1992, A&A, 256, 195
Wood, K., Bjorkman, J. E., Whitney, B., & Code, A. 1996, ApJ, 461, 828 (Paper I)